Available online at www.sciencedirect.com
ScienceDirect
Comput. Methods Appl. Mech. Engrg. 197 (2008) 1397–1409
Computer methods in applied mechanics and engineering
www.elsevier.com/locate/cma

Response classification of simple polycrystalline microstructures

L. Tan [a], S.R. Arwade [b,*]

[a] Johns Hopkins University, Department of Civil Engineering, Baltimore, MD 21218, United States
[b] University of Massachusetts, Department of Civil and Environmental Engineering, 223 Marston Hall, Amherst, MA 01003, United States

Received 30 April 2007; received in revised form 18 October 2007; accepted 14 November 2007
Available online 24 November 2007

Abstract

A new method for approximate solution of mechanics problems is presented that uses a classifier to identify regions in a random heterogeneous material where stress is likely to be highly concentrated under a prescribed set of boundary conditions. The example problem studied is an aggregate of hexagonal grains, each modeled as orthotropic and linear elastic, and subject to uniaxial extension. It is shown that the Sobol' decomposition can be used to determine which surrounding grains mechanical properties play the largest role in determining the average effective stress in any particular grain. It is also shown that the constituent functions of the Sobol' decomposition determine a unique material pattern that corresponds to maximum stress concentration. A reduced order representation of the microstructure is developed that is in essence a projection of the microstructure description onto the material pattern. Finally, a classifier is developed that operates on this reduced order representation to predict the level of stress concentration. This classifier is shown to be over 90% accurate, and, when implemented in a moving window algorithm, to provide very good predictions of the subregions in a large microstructure where large stress concentration is likely.

Keywords: Microstructure; Polycrystal; Probability; Machine learning; Classification

1. Introduction

The simulation of deformation fields in random heterogeneous materials receives ever increasing attention as engineers become more desirous of methods for accurately predicting structural failure modes and designing materials with specific properties. While the majority of research directed at this goal emphasizes the development of solution, or multiscale techniques that allow the more accurate simulation of the response of larger volumes of material, the goal of this work is to develop a new method for identifying locations within large, random, and heterogeneous, solid bodies, that are likely to be sites of stress localization. This new method, based on pattern recognition and classification, does not rely on discretization of the governing equations or the solution of large systems of equations, but delivers approximate predictions of likely localization sites. This method may prove particularly useful within the context of large scale computational approaches by providing guidance as to where in a random heterogeneous body computational resources should be allocated.

Due to the spatial heterogeneity of material properties in polycrystalline materials, analytic solutions for the mechanical response to loads can be obtained only for very specialized cases, such as a single ellipsoidal crystal embedded in an infinite homogeneous medium [1,2] or planar polycrystals with only two slip systems [3]. It is possible to build up approximate solutions for the response of polycrystals using superposition of these analytic solutions, but the approximation is typically large enough that the solutions are only useful for qualitative studies. At this time, the only practical alternative approach to determining polycrystal response is the finite element method [4,5], in which the crystalline geometry is represented explicitly, and appropriate constitutive models such as anisotropic elasticity or singly crystal plasticity are implemented. While such simulations provide high fidelity predictions of the

* Corresponding author. Tel.: +1 413 577 0926.
E-mail address: arwade@ecs.umass.edu (S.R. Arwade).

0045-7825/$ - see front matter © 2007 Elsevier B.V. All rights reserved.
doi:10.1016/j.cma.2007.11.011

response—the stress field for example—the calculations for all but the smallest polycrystals are very time consuming, and even generating high quality meshes for random polycrystalline geometry is a significant challenge. An alternative to these two approaches is to concentrate on the bulk, or homogenized, polycrystal response. An example of this approach is the construction of finite element models of the orientation space [6,7]. Here, the three-dimensional region in which the orientation distribution function (ODF) is defined is discretized into finite elements. The finite element method is used here not to solve the partial differential equations of continuum mechanics, but rather the equations governing the evolution of the ODF in response to inelastic material deformation. This approach has the advantages that the discretized domain, representing the ODF rather than the solid body, does not deform, and is relatively compact, so that the total number of degrees of freedom is not large, and does not increase with the size of the polycrystal being modeled. The results of finite element calculations of ODF evolution are particularly useful in material processing contexts, when the goal is typically to control the bulk material properties. All information regarding the local arrangement of grains in the polycrystal is lost, however, when the problem is transformed to the orientation space, and therefore the method is not appropriate for studying localization phenomena. Some attempts have been made to develop approximate methods for mechanics analysis. Two relevant examples, upon which this work builds, rely on the development of fracture mechanics-based heuristics for crack propagation [8], or the applications of pattern recognition to the mechanics of particle–reinforced composites [9].

This paper describes a new method for studying localization in heterogeneous polycrystals based on pattern recognition and classification techniques primarily developed by computer scientists for use in such applications as face identification. The goal is to identify sites within a heterogeneous polycrystal where localization is likely to occur *without* the use of intensive finite element analysis. In the example application shown here, the polycrystal is assumed to be two-dimensional, each grain is assumed hexagonal, and orthotropic elasticity is assumed within each grain. Localization is taken to mean effective stress concentration within a grain above a threshold effective stress under uniaxial extension. The proposed method can be outlined by the following steps:

(1) Generate random, independent training samples, which are polycrystals that contain a relatively small number of grains, but the size of which is equal to the length scale at which intergranular interactions die out.
(2) Use finite element analysis or some other high fidelity analysis technique to determine the state of stress in these training samples.
(3) Identify patterns in the arrangement of crystal orientations that result in highly concentrated effective stress in the central grain of the training samples.
(4) Reformulate these patterns as basis vectors for a new space in which polycrystals of the same size as the training samples can be represented. This space is called the microstructural feature space.
(5) Derive a classifier in the microstructural feature space for predicting, based on the arrangement of crystal orientations, the degree of effective stress concentration in the central grain.
(6) Implement a moving window technique using the derived classifier to identify sites of likely effective stress concentration in a large polycrystal.

The novelty in this approach comes from the reduced order representation of the microstructure made possible by the basis function derivation (step 4), the application of classifier techniques to mechanics problems (step 5), and the use of a modified version of the Sobol' decomposition of a function of random variables [10,11] to identify the relevant microstructural patterns (step 3).

The presentation of this new method for micromechanics analysis begins with the detailed problem statement. Following is the description of training sample generation and pattern identification using the Sobol' decomposition, which patterns are used in the reduced order description of the polycrystalline microstructure. Next, the classifier is developed that predicts the degree of effective stress concentration, and finally this moving window classification technique is applied to an example polycrystalline microstructure, showing excellent results when compared to a reference finite element simulation.

2. Problem statement and definitions

Consider a two-dimensional polycrystal in which all the grains are regular hexagons of uniform size. A linear elastic orthotropic material model is selected for the intragranular material, with a single angle θ defining the orientation of the crystal principal material axes relative to a reference coordinate system [12–14]. The periodicity of the orthotropic material model, in which $E_x = E_y$, requires only that this orientation angle be defined on the interval $[0, \pi/2) \equiv [0, 90^\circ)$. For illustrative purposes, the properties of single crystal copper are selected with

$$C_{11} = 168{,}000 \text{ MPa}, \quad C_{12} = 121{,}400 \text{ MPa}, \quad C_{44} = 75{,}400 \text{ MPa}. \tag{1}$$

The polycrystal is subject to uniaxial extension in the global y-direction. This displacement field is applied through the use of periodic displacement boundary conditions on the boundary of the polycrystal. Fig. 1 shows an example polycrystal where the greyscale represents the orientation angle.

The deformation field, applied through the displacement boundary conditions on the polycrystal, generates a heterogeneous stress field $\sigma(x)$ throughout the polycrystal. Spatial heterogeneity of the stress field is induced by variation

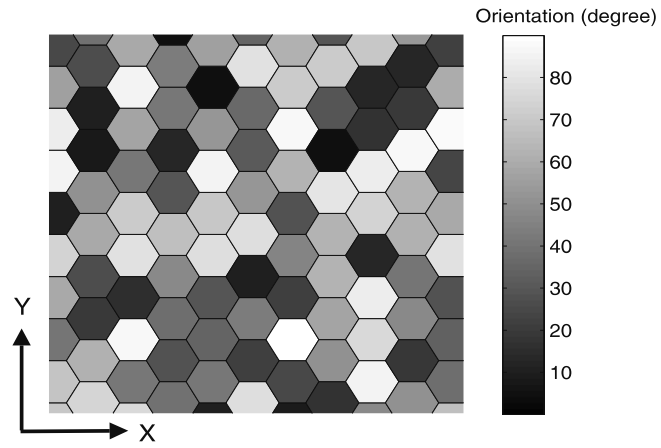

Fig. 1. Two-dimensional material model for the polycrystalline microstructure. Each grain is represented by a regular hexagon and orientations for grains are independent and shown by greyscale.

of the orientation angle among grains, and, by extension, spatial heterogeneity of the material constitutive matrix. Define for each grain in the polycrystal an average effective, or von Mises, stress $s_i = \bar{\sigma}_{\text{eff},i} = \frac{1}{A}\int_{G_i} \sigma_{\text{eff}}(x)\mathrm{d}A$, where G_i represents grain i, $\sigma_{\text{eff}}(x)$ is the effective, or von Mises stress at location $x \in G_i$, and A is the area of G_i. The average effective stress for each grain is the response of interest in this work. Note that this definition neglects variation of the stress field within individual grains, and also does not capture the large stress concentrations—even singularities—that can occur due to the elastic mismatch at grain boundaries. Because the goal of this work is to identify the location of stress concentration only within approximately one grain diameter, however, these smaller scaler fluctuations can be ignored. It would, however, be straightforward to address these smaller scale fluctuations without making major changes to the method. Given this statement of the problem geometry, material model, and boundary conditions, the goal is to use pattern recognition and a classifier to predict which grains in a large polycrystal will meet the condition $s_i > s^*$, where s^* is a threshold stress level. These sites are closely related to the locations where damage could be expected to occur in the polycrystal if a stress-based damage criterion is appropriate.

3. Generation of training data and classifier definition

The classifier introduced in this section attempts to connect the average effective stress in a grain to the orientations of its neighbor grains under a specified set of boundary conditions as described above. In order to identify mechanically relevant patterns in the microstructure, and train the classifier, a set of training data is required. In this case, a training sample is an aggregate of a relatively small number of grains for which the stress state resulting from the imposed boundary conditions has been determined by a high fidelity simulation (FEA for example). The training samples used here consist of aggregates of 61 grains (Fig. 2) in which the orientations are independently generated, and uniformly distributed in $[0, \pi/2)$. The size of the training samples is guided by the exact solutions for a circular orthotropic inclusion in an infinite medium, which shows that the local interactions become insignificant over a distance approximately equal to four times the inclusion diameter. Therefore, the training samples are large enough to include the fourth nearest neighbors of the central grain.

To make the generation of training samples somewhat more efficient, the stress fields in 100-grain polycrystals are calculated using a high fidelity simulation. In this case, a triangular spring network model with material properties calibrated to the orthotropic crystal properties is used, rather than a continuum finite element model. The density of the spring network is such that each grain contains approximately 100 elements, providing sufficient resolution of the state of stress within each grain. From this 100-grain aggregate, four 61-grain training samples are extracted. These four training samples overlap to some degree, meaning that the training samples are not independent from one another. This effect is considered to be small, however, since a total of 15,968 61-grain training samples are generated from 3992 100-grain aggregates.

The training samples provide samples of the microstructural response function $s_1(\theta_1, \theta_2, \ldots, \theta_{61})$ which gives the average effective stress in grain 1 as a function of the orientation angles in grain 1 and its 60 nearest neighbors. The high dimensionality of the space in which the microstructural response function is defined precludes the development of an efficient classifier or the use of response

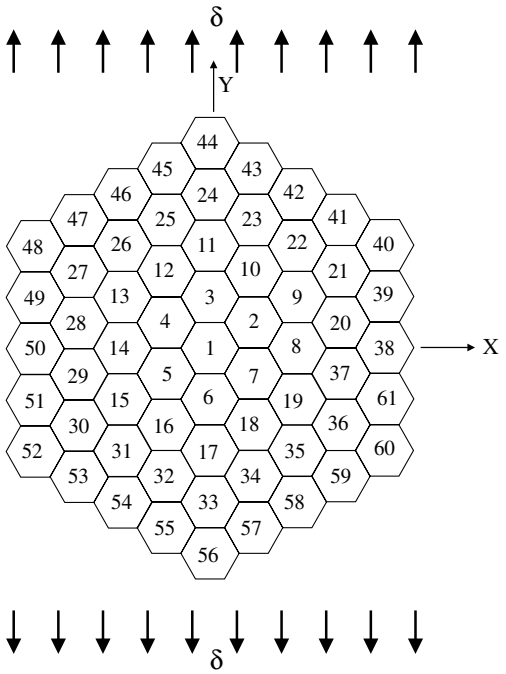

Fig. 2. Sixty-one-grain polycrystalline aggregate showing grain numbering scheme and remote boundary conditions.

surface type approaches. Therefore, as a preliminary to the development of a classifier for the average effective stress, a procedure is introduced for identifying mechanically meaningful patterns in the microstructure. These patterns are then used to form a reduced order description of the microstructure of dimension small enough that efficient classification is possible. In this application, the pattern identification is made using the Sobol' decomposition of a function of many random variables, and consists of (1) the identification of the subset of the 60 nearest neighbor grains the orientation of which significantly affects the magnitude of s_1 and (2) the orientation values in these grains that tend to result in elevated values of s_1. Here, one pattern, corresponding to elevated s_1 suffices, and so the reduced order microstructural description is one-dimensional, and the resulting classifier is a very simple one, with one node and two leaves. If the reduced order description is given by $\alpha(\theta_1, \theta_2, \ldots, \theta_{61})$, then the classifier can be expressed as

$$C(\alpha) \approx C(\theta_1, \theta_2, \ldots, \theta_{61}) = \begin{cases} \text{critical} \\ \text{non-critical} \end{cases} \tag{2}$$

where 'critical' is interpreted to mean that the condition $s_1 > s^*$ is met, and 'non-critical' is complementary to this definition. The approximation results because, as will be seen in the following sections, the inverse mapping from the reduced order description α to the full representation $(\theta_1, \theta_2, \ldots, \theta_{61})$ is not unique.

4. Pattern extraction using the Sobol' representation

The microstructure response function $s(\theta_1, \theta_2, \ldots, \theta_{61})$ can be viewed as a function of 61 random variables that are, in this case, independent. Note that the subscript on s has been dropped since hereafter only the stresses in the central grain of a 61-grain neighborhood are of interest. The challenge in identifying a mechanically relevant pattern among these 61 variables consists of both identifying which of the variables should be considered part of the pattern, and what values they take. Here these twin goals are accomplished through a novel application of the Sobol' decomposition of multivariate functions [10,11]. A review of this decomposition is first given, followed by an extension to make it useable in the current context, and finally it is shown how the Sobol' indices can be used to select the subset of important input variables, and the Sobol' functions used to set the values of those variables.

4.1. Sobol' representation and Sobol' indices

This section presents a brief overview of the relevant features and definitions of the Sobol' decomposition. The details underlying these statements are to be found in [10,11]. Consider a square integrable scalar function $y = f(x)$ of n input random variables contained in $x \in U^n$, where U^n is the unit hypercube, and the elements of x are assumed to be independent.

The Sobol' representation of $f(x)$ is

$$\begin{aligned} f(x) &= f_0 + \sum_{m=1}^{n} \sum_{i_1 < \cdots < i_m} f_{i_1 \cdots i_m}(x_{i_1}, \ldots, x_{i_m}) \\ &= f_0 + \sum_{i=1}^{n} f_i(x_i) + \sum_{i<j} f_{ij}(x_i, x_j) \\ &\quad + \cdots + f_{12\cdots n}(x_1, \ldots, x_n). \end{aligned} \tag{3}$$

The terms of this expansion are defined so that

$$f_0 = \int_{U^n} f(x)\mathrm{d}x \tag{4}$$

is the mean value of $f(x)$,

$$f_i(x_i) = \int_{U^{n-1}} f(x) \prod_{p \neq i} \mathrm{d}x_p - f_0 \tag{5}$$

are the first order terms, obtained by integration with respect to all but one of the variables, and

$$f_{ij}(x_i, x_j) = \int_{U^{n-2}} f(x) \prod_{p \neq i,j} \mathrm{d}x_p - f_i(x_i) - f_j(x_j) - f_0 \tag{6}$$

are the second order terms, obtained by integration over all but two of the variables. The higher order terms are defined analogously. The Sobol' decomposition has many useful properties that are defined in detail in the references, but are peripheral to the application described here, and so are omitted. Only those properties made use of herein are now described.

Considering, as defined above, that the elements of x are independent, the variance of $f(x)$ is

$$D = \int_{U^n} f^2(x)\mathrm{d}x - f_0^2, \tag{7}$$

which can be decomposed into partial variances

$$D = \sum_{m=1}^{n} \sum_{i_1 < \cdots < i_m} D_{i_1 \cdots i_m} \tag{8}$$

$$= \sum_{i=1}^{n} D_i + \sum_{i<j} D_{ij} + \cdots + D_{12\cdots n} \tag{9}$$

in which the individual terms follow the definition

$$D_{i_1 \cdots i_m} = \int_{U^m} f^2_{i_1 \cdots i_m}(x_{i_1}, \ldots, x_{i_m})\mathrm{d}x_{i_1 \ldots} x_{i_m}. \tag{10}$$

The Sobol' indices are the partial variances expressed as fractions of the total variance, namely,

$$S_{i_1 \cdots i_m} = D_{i_1 \cdots i_m}/D. \tag{11}$$

These indices quantify the contribution to the total variance of the individual input variables and all possible combinations of input variables.

4.2. Extension of Sobol' representation

In the problem addressed here, $f(x)$ is replaced by $s(\theta_1, \theta_2, \ldots, \theta_{61})$, where the input variables are the material orientations of the grains. This microstructural response function is decomposed into its constituent Sobol' functions, and the corresponding Sobol' indices are calculated. The Sobol' indices define which of the 61 orientation variables should be retained in a reduced order description of the microstructure, and the Sobol' functions define the values of these variables that will be used in defining a pattern corresponding to microstructure criticality, that is, elevated effective stress in the central grain.

A small modification is required to apply the Sobol' decomposition to this problem because the orientations are not uniformly distributed in the unit hypercube. Rather, the orientations $\{\theta_i\}$ are uniform on the interval $[0, \pi/2)$, and are independent. Extending the Sobol' decomposition to account for this change in input variable distribution is straightforward, and the key steps are given here.

The microstructure response function can be written

$$\begin{aligned} s &= s\left(\frac{\pi}{2}y_1, \frac{\pi}{2}y_2, \ldots, \frac{\pi}{2}y_{61}\right) \\ &= f(y_1, y_2, \ldots, y_{61}) \end{aligned} \tag{12}$$

by using the change of variables $y_i = 2\theta_i/\pi$, resulting in $y_i \sim U(0,1)$.

The Sobol' representation of s is, therefore,

$$\begin{aligned} s &= f(y_1, y_2, \cdots, y_{61}) \qquad (13)\\ &= f_0 + \sum_{m=1}^{61} \sum_{1 \leqslant i_1 < \cdots < i_m \leqslant 61} f_{i_1 \cdots i_m}(y_{i_1}, \ldots, y_{i_m}) \\ &= s_0 + \sum_{m=1}^{61} \sum_{1 \leqslant i_1 < \cdots < i_m \leqslant 61} s_{i_1 \cdots i_m}(\theta_{i_1}, \ldots, \theta_{i_m}), \qquad (14) \end{aligned}$$

where

$$\begin{aligned} s_0 &= f_0 \\ &= \int_{U^{61}} f(y_1, y_2, \ldots, y_{61}) \prod_{j=1}^{61} \mathrm{d}y_j \qquad (15)\\ &= \int_{\left(\frac{\pi}{2}U\right)^{61}} s(\theta_1, \theta_2, \ldots, \theta_{61}) \left(\frac{2}{\pi}\right)^{61} \prod_{j=1}^{61} \mathrm{d}\theta_j \\ &= E_{\theta_1 \theta_2 \cdots \theta_{61}}[s(\theta_1, \theta_2, \ldots, \theta_{61})] \qquad (16) \end{aligned}$$

and

$$\begin{aligned} s_i(\theta_i) &= f_i(y_i) \qquad (17)\\ &= \int_{U^{n-1}} f(x) \prod_{p \neq i} \mathrm{d}y_p - f_0 \\ &= \int_{\left(\frac{\pi}{2}U\right)^{n-1}} s(\theta) \left(\frac{2}{\pi}\right)^{60} \prod_{p \neq i} \mathrm{d}\theta_p - s_0 \\ &= E_{\theta_1 \theta_2 \cdots \theta_{i-1} \theta_{i+1} \cdots \theta_{61}}[s(\theta_1, \theta_2, \ldots, \theta_{61})] - s_0. \end{aligned}$$

The second order terms are given by

$$s_{ij}(\theta_i, \theta_j) = E_{\substack{\theta_1 \cdots \theta_p \cdots \theta_{61} \\ p \neq i,j}}[s(\theta_1, \theta_2, \ldots, \theta_{61})] - s_i(\theta_i) - s_j(\theta_j) - s_0. \tag{18}$$

In the above expressions, $E[\cdot]$ is the expectation operator and $\left(\frac{\pi}{2}U\right)^n$ is a hypercube of dimension n with side length $\pi/2$. These expressions make clear that the integrals used in defining the Sobol' decomposition are simply expectations. When the input variables are uniform, but defined on an interval other than $[0,1)$, the marginal probability density functions must appear explicitly in the integral expressions. The use of the expectation notation provides a simple way to write the variance, partial variances, and Sobol' indices for the microstructure response function, namely,

$$\begin{aligned} D &= E_{\theta_1 \cdots \theta_p \cdots \theta_{61}}[s^2] - s_0^2, \qquad (19)\\ D_{i_1 \cdots i_m} &= E_{\theta_1 \cdots \theta_m}[s^2_{\theta_1 \cdots \theta_m}], \\ S_{i_1 \cdots i_m} &= D_{i_1 \cdots i_m}/D. \end{aligned}$$

These definitions apply as long as the input variables are uniform and independent. When the variables are dependent, or non-uniform, further modifications to the Sobol' decomposition are required. This extension is a topic of current research by the authors.

4.3. Calculation of Sobol' quantities by Monte Carlo simulation

The analytic expressions for the Sobol' functions and indices rely on integration of the microstructure response function. In the current application, the form of $s(\theta_1, \theta_2, \ldots, \theta_{61})$ is not known. The integrals needed to evaluate the Sobol' functions and indices are therefore computed by Monte Carlo simulation using the training data described above. Only the first order terms of the decomposition are calculated here, and it is shown in the following sections that this is sufficient to identify the mechanically relevant pattern in the material microstructure.

The training set consists of N samples, for each of which the spring network analysis provides a single evaluation $s^{(j)}(\theta_1^{(j)}, \theta_2^{(j)}, \ldots, \theta_{61}^{(j)})$, which is the average effective stress in grain 1 of training sample j. These data points provide the first order Sobol' functions according to

$$\begin{aligned} s_0 &= \frac{1}{N} \sum_{j=1}^{N} s^{(j)}(\theta_1^{(j)}, \theta_2^{(j)}, \ldots, \theta_{61}^{(j)}) \\ s_i(\hat{\theta}_k) &= \frac{1}{\sum_{j=1}^{N} I_{[\hat{\theta}_k - \Delta\theta \leqslant \theta_i^{(j)} < \hat{\theta}_k + \Delta\theta]}} \sum_{j=1}^{N} I_{[\hat{\theta}_k - \Delta\theta \leqslant \theta_i^{(j)} < \hat{\theta}_k + \Delta\theta]} \\ &\qquad s^{(j)}(\theta_1^{(j)}, \theta_2^{(j)}, \ldots, \theta_n^{(j)}) - s_0 \end{aligned} \tag{20}$$

in which $I_{[\cdot]}$ is an indicator function, and $\{\hat{\theta}_k\}$ are a set of N_k values evenly spaced in the interval $[0, \pi/2)$ at which the first order Sobol' functions are estimated. The variance

and partial variances of the microstructure response function are calculated by

$$D = \frac{1}{N}\sum_{j=1}^{N} s(\theta_1^{(j)}, \theta_2^{(j)}, \ldots, \theta_n^{(j)})^2 - s_0^2,$$

$$D_i = \frac{1}{N_k}\sum_{k=1}^{N_k} s_i(\hat{\theta}_k)^2. \tag{21}$$

In the current example, the number of training samples is $N = 15,968$, and the number of orientation intervals is $N_k = 90$, yielding $\Delta\theta = \pi/180$ and $\hat{\theta}_k = k\pi/90 + \pi/180$, $k = 0, 1, \ldots, 90$.

4.4. Pattern identification using the Sobol' decomposition

The symmetry of the grain geometry in the example problem is exploited to effectively increase the number of training samples and thereby reduce the estimation error inherent in the evaluation of expressions (20) and (21). Define a 19-grain model according to Fig. 3 with orientations denoted by $\{\theta_i^*\}$ with $i = 1, 2, \ldots, 19$. By using the orientations of the 19-grain model, a four-fold increase is achieved in the number of training samples available for evaluation of $s_i^*(\theta_i^*)$ for $i = [2, 5, 6, 8, 9, 10, 11, 14, 15, 16, 17, 18]$ (group 1), and a two-fold increase for $i = [3, 7, 12, 19]$ (group 2) and $i = [4, 13]$ (group 3). The number of samples available when $i = 1$ is unchanged. Problem symmetry dictates the following example relationships: $\theta_2^* \equiv \theta_2 \equiv \pi/2 - \theta_4 \equiv \theta_5 \equiv \pi/2 - \theta_7$ for group 1; $\theta_3^* \equiv \theta_3 \equiv \theta_6$ for group 2; $\theta_4 \equiv \theta_8 \equiv \pi/2 - \theta_{14}$ for group 3.

It is emphasized that the symmetry referred to above is not present in the actual material properties. For example, in a given training sample, $\theta_1 \neq \theta_6$, so that the symmetry referred to is not the classical symmetry of mechanics in which only a single quadrant of a doubly symmetric domain with doubly symmetric boundary conditions must be analyzed. What is taken advantage of in this application example is simply the symmetry in the grain geometry. For example, intuition suggests that θ_2 and θ_5 should have the same influence on s, and that the values of θ_2 and θ_5 that maximize s should be equal. Preliminary analysis not shown here indicates the validity of this intuition, in that $s_2 \approx s_5$, and $s_2(\theta_2) \approx s_5(\theta_5)$. Thus, the symmetry used here results simply in an increase in the number of samples available for estimating the Sobol' indices and functions, and does not impose or presuppose any constraints on the deformations or arrangement of material properties in the polycrystal. If the geometric symmetry of the grains is broken, by, for example, the introduction of spatially varying grain size, the only modification to the procedure described here is that more training samples must be generated to estimate the Sobol' indices and functions.

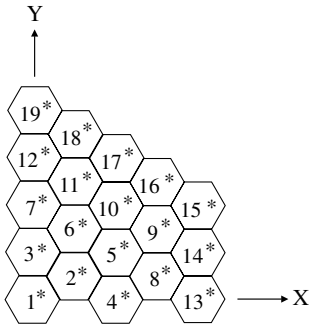

Fig. 3. Nineteen-grain polycrystalline aggregate derived using symmetry conditions on 61-grain aggregate.

Using expressions (20) and (21), modified appropriately to take advantage of the symmetry expressions above, the first order Sobol' functions and indices are estimated from the training samples. Each of these functions $s_i^*(\theta_i^*)$, $\theta_i^* \in [0, \pi/2)$ represents, approximately, the dependence of the microstructural response $s(\theta_1, \theta_2, \ldots, \theta_{61})$ on each of the individual input variables, making use of the symmetry relationships above so that, for example, $s_2(\theta_2) \equiv s_4(\pi/2 - \theta_4) \equiv s_5(\theta_5) \equiv s_7(\pi/2 - \theta_7) \equiv s_2^*(\theta_2^*)$, and likewise for the other groups of grains. The Sobol' indices require no transformation so that $S_2 = S_4 = S_5 = S_7 = S_2^*$, and likewise for the other groups. Table 1 shows the full set of equivalences between the 19- and 61-grain models.

Fig. 4 shows the Sobol' indices calculated for the 19-grain model. Note that $\log_{10}(S_i^*)$ is shown because of the very large range of magnitudes of S_i^*. These results quantify the intuitive prediction that the orientation of grains close to the center of the neighborhood, and aligned with the global y-axis (the loading axis) have more effect on the state of stress in the central grain. For example, $S_7^* \gg S_4^*$, even though they are both second nearest neighbors to grain 1, and $S_2^* \gg S_{19}^*$ although they both lie along the global y-axis. Also, since $\sum_{i=1}^{19} S_i^* \approx 1$, it is confirmed that the 61-grain model, represented here by the 19-grain model, contains a sufficient volume of material to capture nearly all of the heterogeneity of material properties that influence the

Table 1
Correspondence between 19-grain model and 61-grain model

Equivalent grain of 19-grain model	Grains of 61-grain model			
1*	1			
2*	2	4	5	7
3*	3	6		
4*	8	14		
5*	9	13	15	19
6*	10	12	16	18
7*	11	17		
8*	20	28	29	37
9*	21	27	30	36
10*	22	26	31	35
11*	23	25	32	34
12*	24	33		
13*	38	50		
14*	39	49	51	61
15*	40	48	52	60
16*	41	47	53	59
17*	42	46	54	58
18*	43	45	55	57
19*	44	56		

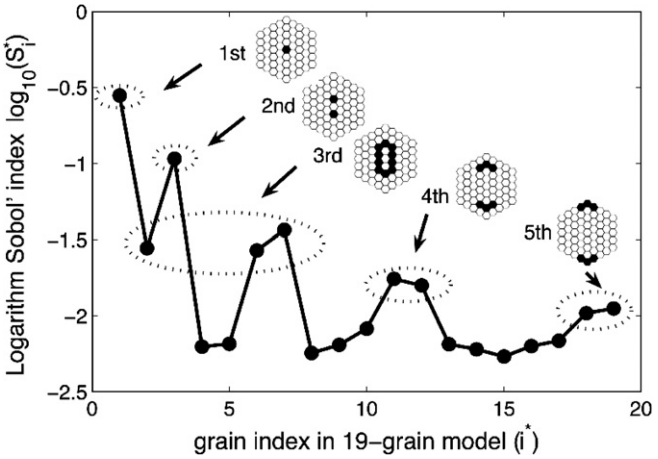

Fig. 4. Sobol' indices for orientations of the 19-grain model. Darkened grains in the insets indicate the locations of the grains with relatively large Sobol' indices. All of the grains for which $\log S_i > -2$ are selected as significant to determining the stress in the central grain, and are separated into five groups, or patterns. The groups are chosen based on clustering of the Sobol' indices.

stress state in the central grain. It is possible to identify within Fig. 4 five groups of grains with similar Sobol' indices, and that have Sobol' indices substantially larger than for grains not in one of these five groups. These groupings are identified visually, and are denoted the first through fifth geometric patterns of the microstructure where the numbering is applied in decreasing order of Sobol' index magnitude. The inset figures show the locations of the grains in each of the five groups, and Fig. 5 shows how the five groups of grains are arranged in the 61-grain neighborhood, along with the limiting values of S_i^* for each of the groups. Note that while the patterns agree with intuition in a general way, their determination via the Sobol' indices is systematic, could be readily applied to more subtle problems, and provides some results that are not immediately obvious. For example, intuition may not lead an analyst to conclude that θ_2^* and θ_7^* are very nearly equally important in controlling the central grain stress state. Table 2 shows which grains of the 19-grain and corresponding 61-grain model are involved in each of the geometric patterns using a notation in which the sets of grains in the microstructural patterns are denoted by $I_k \subset \{1, 2, \ldots, 61\}$. For example, $I_2 = \{3, 6\}$ and $I_4 = \{23, 24, 25, 32, 33, 34\}$.

Having used the Sobol' indices to identify the grains that contribute significantly to determining the state of stress in the central grain, and assigning these grains to groups, or geometric patterns, based on the magnitude of their influence on s, the first order Sobol' functions corresponding to the orientation of these grains are used to determine the values that will form the pattern of material properties used in classification. Fig. 6 shows the estimated Sobol' functions for 4 of the orientations in the 19-grain model. For each Sobol' function there exists a unique $\theta_{i,\max}^* \in [0, \pi/2)$ satisfying

$$\theta_{i,\max}^* = \arg\max_{\theta_i^* \in [0,\pi/2)} [s_i^*(\theta_i^*)]. \tag{22}$$

These are the values of the grain orientations in the 19-grain model that tend to increase s. These stress maximizing orientations are shown in Fig. 7. The orientations, combined with the geometric patterns described above, form a set of five microstructural patterns $\{\phi_i\}$ that are related to the state of stress in the central grain. It is emphasized that these patterns have been determined in a systematic way by analyzing the microstructure response

Table 2
Grains involved in geometric patterns

Rank	Constituent grains from 19-grain model	Constituent grains from 61-grain model (I_k)
1	1^*	1
2	3^*	3,6
3	2^*,6^*,7^*	2,4,5,7,10,11,12,16,17,18
4	11^*,12^*	23,24,25,32,33,34
5	18^*,19^*	43,44,45,55,56,57
6	Other	Other

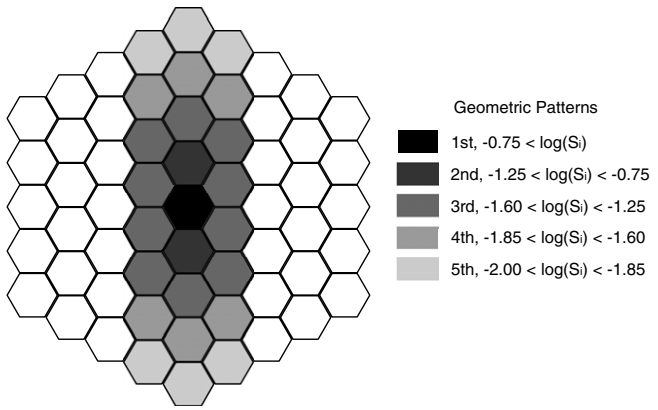

Fig. 5. Geometric patterns in 61-grain model. Greyed grains are those for which $\log(S_i) > -2$, indicating a significant influence on the stress of the central grain. The grey scale corresponds to the magnitude of the Sobol' indices so that the darker grains have larger influence on the stress in the central grain.

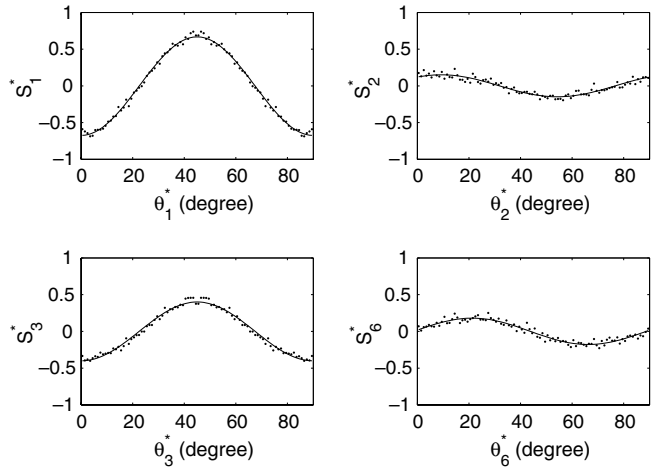

Fig. 6. Six first order terms of Sobol' representation. Points are estimated from training data and solid lines are the best fit trigonometric functions.

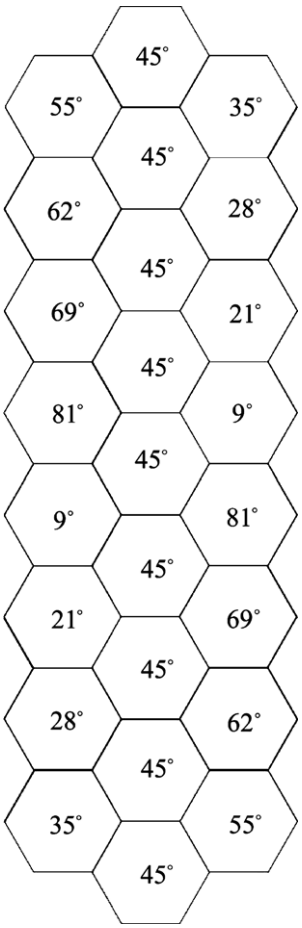

Fig. 7. Grain orientations $\theta_{i,\max}$ that maximize the corresponding first order Sobol' functions.

function using the Sobol' decomposition. This procedure can be readily extended to more complicated microstructures or general stochastic mechanics problems. In the following sections the microstructural patterns are used to form a reduced order description of the microstructure, and this reduced order description is then used in a classification scheme that predicts the stress state in a grain without the need for a high fidelity mechanics simulation.

In summary, the patterns that are used to perform classification consist of two parts, the geometry, or location of the contributing grains, and the material properties, or grain orientations that maximize the central grain stress s. The geometric part of the pattern is found using the Sobol' indices, and the material property part is found using the Sobol' functions. In this particular application, the pattern is divided into five sub-patterns, or groups, so that different weights can be assigned to input variables (grain orientations) with different magnitudes of influence on the central grain stress s.

5. Classification of the microstructural response

The results of the previous section are used to develop a reduced order description of the 61-grain microstructural model. A classifier is then developed that operates on this reduced order description to provide predictions of $s(\theta_1, \theta_2, \ldots, \theta_{61})$.

5.1. Reduced order microstructural representation

The raw representation of the 61-grain microstructure is simply the 61 dimensional vector of orientations in each of the grains $[\theta_1, \theta_2, \ldots, \theta_{61}]$. Here, the reduced order representation is defined as

$$[\psi_1, \psi_2, \ldots, \psi_5] = \Gamma(\theta_1, \theta_2, \ldots, \theta_{61}). \tag{23}$$

The elements on the left-hand side of Eq. (23) represent projections of the orientations $\{\theta_1, \ldots, \theta_{61}\}$ onto the microstructural patterns $\{\phi_1, \ldots, \phi_5\}$ and form the coordinates of a five-dimensional representation of the 61-grain model. The function $\Gamma(\theta_1, \theta_2, \ldots, \theta_{61})$ represents a form of projection of the 61 orientations onto the five microstructural patterns that is not a standard vector projection, but is specially defined here in response to the form of the 61 input variables and the microstructural patterns. The mapping from the 61 to five-dimensional spaces represented by $\Gamma(\theta_1, \theta_2, \ldots, \theta_{61})$ is many-to-one, meaning that any attempt to classify the microstructural response using the reduced order coordinates $(\psi_1, \ldots, \psi_5)$ will be approximate.

The definition of the dimension reduction projection of Eq. (23) is constructed using a complex transformation of the raw microstructural variables $\{\theta_i\}$ that accounts for the $\pi/2$ periodicity of the orientation. Define

$$G(\theta_i) = \mathrm{e}^{\mathrm{i}(4\theta_i)}, \tag{24}$$

where $\mathrm{i} = \sqrt{-1}$ when not appearing as an index. This transformation overcomes the difficulty, among others, that the interval $[0, \pi/2)$ is not closed to addition and subtraction operations. This complex transformation of the orientation angles allows a straightforward definition of the projection operation needed to calculate Eq. (23). The projection of the vector of orientations $[\theta_1, \theta_2, \ldots, \theta_{61}]$ onto the microstructural patterns is defined by

$$\psi_j(\theta_1, \theta_2, \ldots, \theta_{61}) = \mathrm{Re}\left\{ \sum_{k \in I_j} \mathrm{e}^{-4\mathrm{i}\theta_{k,\max}} \cdot \mathrm{e}^{4\mathrm{i}\theta_k} \right\}, \tag{25}$$

providing a scalar measure of how close the actual orientations are to the maximizing orientations. The quantities ψ_j are maximized when the orientations in a particular aggregate of grains exactly match the pattern that maximizes stress, namely that shown in Fig. 7. Conversely, they are minimized when the orientations differ from those shown in the pattern by $\pi/4$. Because the material is orthotropic with a constitutive matrix that is unchanged by rotations of multiples of $\pi/2$, this projection effectively measures how close the stiffnesses of the grains in an aggregate are to the stiffnesses of the grains in the pattern. Results shown later (Fig. 8) demonstrate that the response increases monotonically, in an average sense, with the parameters ψ_j.

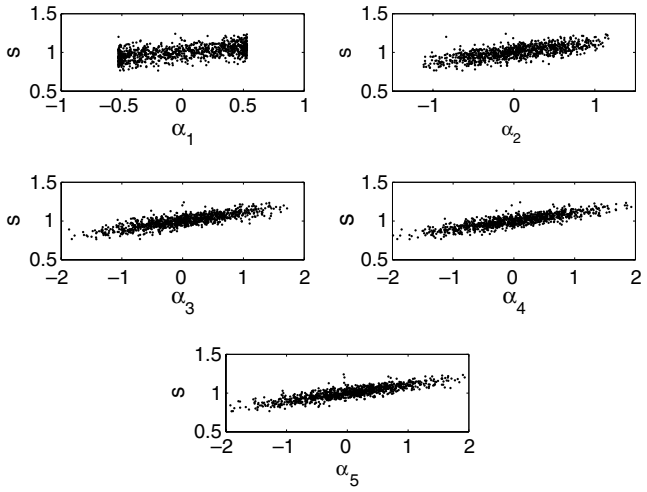

Fig. 8. Training samples and normalized response represented in the one-dimensional space defined by α_k.

It would be possible to develop a classifier for s in the five-dimensional space defined by the pattern projection coefficients $\{\psi_i\}$. Here, however, the coefficients are further combined to provide a single scalar measure of the proximity of the microstructure orientations to their maximizing values. This further dimension reduction is accomplished by a weighted sum of the individual pattern projection coefficients, namely,

$$\alpha_k = \sum_{j=1}^{k} w_j \psi_j, \quad k = 1, \ldots, 5. \tag{26}$$

Here, the weights are denoted by $\{w_j\}$, and the parameter k controls how many of the microstructural patterns participate in determining α_k. If k is larger, more grain orientations are considered in the calculation. The weights are determined according to

$$w_j = \frac{1}{\sum_{i=1}^{61} I_{[i \in I_j]}} \sum_{i=1}^{61} I_{[i \in I_j]} \sqrt{S_i} \tag{27}$$

representing the average square root Sobol' index for all the grains in microstructural pattern j. Thus, the patterns containing grains that are more important in determining s, the average effective stress in the central grain, also play a large role in determining the value of α_k, the scalar representation of the microstructural orientations.

Fig. 8 shows the average effective stress in the central grain of the training samples plotted against α_k. From the definition of α_k and consultation with the figure, one can see that large values of α_k derive from microstructures with orientations that are close to the maximizing microstructural patterns, and, therefore, correspond to elevated values of s. Also, the scatter in the relationship between α_k and s decreases substantially as k increases, reflecting the inclusion of additional microstructural information in the calculation of α_k. In the next section a classifier based on the data of Fig. 8 is developed and tested.

By defining α_k as above, the number of dimensions needed to describe the microstructure has been reduced from 61 to 1. This is a dramatic reduction in the number of variables needed to describe the microstructure, but it is shown in the following sections that it is possible to develop a classifier using this scalar microstructural descriptor that delivers satisfactory accuracy in predicting the stress in the individual grains of a polycrystal. This success may be due in part to the relative simplicity of the microstructural geometry, response, and boundary conditions considered here—regular hexagons, linear elastic deformation, uniaxial extension. In more general micromechanics problems it may be necessary to use an intermediate number of variables for microstructural description.

5.2. Definition of microstructural classifier

Here it is shown that a very simple classifier can be developed to predict the average effective stress in a grain of a polycrystal using a scalar representation of the orientation of neighboring grains. The classifier has the form

$$\begin{aligned} C(\alpha_k) &\approx C(\psi_1, \ldots, \psi_5) \\ &\approx C(\theta_1, \ldots, \theta_{61}) = \begin{cases} \text{critical}, & s > s^* \\ \text{non-critical}, & s \leqslant s^* \end{cases} \end{aligned} \tag{28}$$

The threshold stress is defined by $s^* = \mu_s + \sigma_s$, where μ_s and σ_s are the mean and standard deviation of the average effective stress in all grains of the training samples. In this example the choice of the threshold value is essentially arbitrary. In an actual application, the threshold value of the response function would be chosen based on the specific mechanics. Example choices could be the yield stress, or an effective strain associated with the onset of void growth and damage, with appropriate safety factors accounted for.

The form of the approximate classifier $C(\alpha_k)$ defined above is

$$C_k(\alpha_k) = \begin{cases} \text{critical}, & \alpha_k > \alpha_k^* \\ \text{non-critical}, & \alpha_k \leqslant \alpha_k^* \end{cases} \tag{29}$$

corresponding, in the vocabulary of classification and pattern recognition to a decision tree with a single root node and two leaves. Here, the values α_k^* correspond to the threshold stress values s^*. In the following it is described how α_k^* is selected to minimize the loss associated with classifier error. Although this is the simplest possible decision tree, it is sufficient in this case to illustrate the application of Sobol' decomposition derived patterns to micromechanics problems and a method for incorporating a loss function other than the standard 0–1 loss function into the derivation of the classifier.

The choice of α_k^* is made so as to minimize the loss, or error, of the classifier. The classification result falls into one of four categories defined by Table 3 in which the notation critical $\equiv 1$ and non-critical $\equiv 0$ has been used for compactness.

Table 3
Types of classification result, 1 = critical

	$C_k(\alpha_k) = 1$	$C_k(\alpha_k) = 0$
$C(\theta_1, \ldots, \theta_{61}) = 1$	True positive	False negative
$C(\theta_1, \ldots, \theta_{61}) = 0$	False positive	True negative

For a set of data classified according to Eq. (29) let $n_{\mathrm{TP}}, n_{\mathrm{TN}}, n_{\mathrm{FN}}$ and n_{FP} denote the number of samples that are true positive, true negative, false negative and false positive, respectively. The total accuracy of the classifier $C_k(\alpha_k)$ is

$$\mathrm{Accu}(C_k) = \frac{n_{\mathrm{TP}} + n_{\mathrm{TN}}}{n_{\mathrm{TP}} + n_{\mathrm{TN}} + n_{\mathrm{FN}} + n_{\mathrm{FP}}}. \tag{30}$$

The true positive and true negative rates of the classifier $\mathrm{TP}(C_k)$ and $\mathrm{TN}(C_k)$, are

$$\mathrm{TP}(C_k) = \frac{n_{\mathrm{TP}}}{n_{\mathrm{TP}} + n_{\mathrm{FN}}} \tag{31}$$

and

$$\mathrm{TN}(C_k) = \frac{n_{\mathrm{TN}}}{n_{\mathrm{TN}} + n_{\mathrm{FP}}} \tag{32}$$

and the error rates, the false negative and false positive rates are

$$\mathrm{FN}(C_k) = \frac{n_{\mathrm{FN}}}{n_{\mathrm{TP}} + n_{\mathrm{FN}}} = 1 - \mathrm{TP}(C_k) \tag{33}$$

and

$$\mathrm{FP}(C_k) = \frac{n_{\mathrm{FP}}}{n_{\mathrm{TN}} + n_{\mathrm{FP}}} = 1 - \mathrm{TN}(C_k). \tag{34}$$

Fig. 9 shows the dependence of the total accuracy $\mathrm{Accu}(C_k)$ on α_k^* for each value of k. A well-defined peak in the accuracy occurs for all values of k except $k = 1$, and $\mathrm{Accu}(C_k) > \mathrm{Accu}(C_{k-1})$, although it is not a general results that the inclusion of more independent variables will increase classifier accuracy. It is emphasized that the calculation of the curves of Fig. 9, accomplished by repeated evaluation of Eq. (29), is extremely fast.

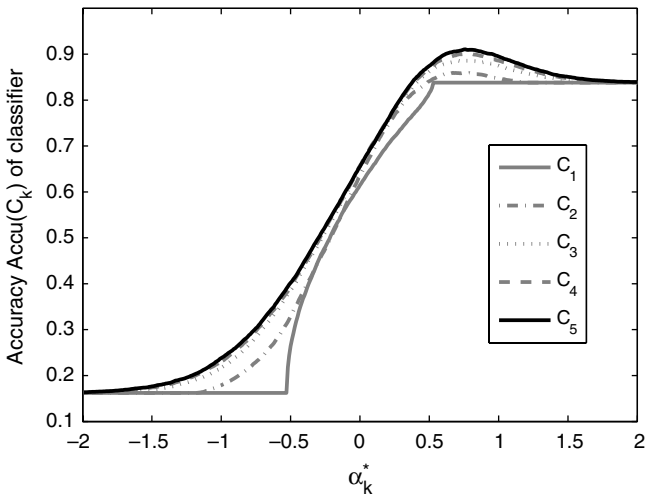

Fig. 9. Classifier accuracy as a function of threshold value α_k^*.

For the classifier C_5, which uses all five of the microstructural patterns, the peak accuracy occurs at $\alpha_5 = 0.76$ giving a total accuracy of $\mathrm{Accu}(C_5) = 0.91$ and the confusion matrix of Table 4, in which C_5^* denotes the classifier $C(\alpha_5)$ with $\alpha_5^* = 0.76$. Selection of α_k^* based on total accuracy represents a compromise between maximizing the true positive and true negative rates, since $\lim_{\alpha_k^* \to -\infty} \mathrm{TP}(C_k) = 1$ and $\lim_{\alpha_k^* \to \infty} \mathrm{TN}(C_k) = 1$. In an engineering context, choosing a low value for α_k^* can be viewed as conservative, resulting in a high true positive rate, but also a high false positive rate. Since a major goal of this work is to make micromechanics analysis more efficient by quickly identifying regions in which localization is likely to occur, such a conservative approach severely limits any possible gains in efficiency. Note here that the confusion matrices presented are based on training accuracy. For the C_5^* classifier, 10-fold cross validation yields a confusion matrix that differs from that of Table 4 by less than one-tenth of 1%. From here forward confusion matrices represent training accuracy.

The definition of accuracy presented above implicitly assigns equal cost to the false positive and false negative errors. This may not be appropriate for engineering applications in which a false negative error, which is unconservative and may compromise safety, is a worse error than a false positive error, which compromises efficiency but not safety. To allow the analyst to properly account for the relative importance of false negative and false positive error, the definition of Eq. (30) is augmented with a parameter c_{FN}, the cost of a false negative error, to give

$$\mathrm{Accu}^c(C_k) = \frac{c_{\mathrm{FN}} n_{\mathrm{TP}} + n_{\mathrm{TN}}}{c_{\mathrm{FN}} n_{\mathrm{TP}} + n_{\mathrm{TN}} + c_{\mathrm{FN}} n_{\mathrm{FN}} + n_{\mathrm{FP}}}. \tag{35}$$

Here the cost of a false positive error is fixed at $c_{\mathrm{FP}} = 1$, which does not cause any loss of generality since only the ratio $c_{\mathrm{FN}}/c_{\mathrm{FP}}$ affects the results. The accuracy function of Eq. (35) can be derived directly from the standard loss function approach to classifier optimization, and therefore the two sets of terms are equivalent. The accuracy vocabulary is adopted here because in the authors opinion it is more readily interpreted in an engineering context than the more abstract loss function vocabulary.

Fig. 10 shows the accuracy curves $\mathrm{Accu}^c(C_k)$ with $c_{\mathrm{FN}} = 1.5$. For $k = 5$ the peak accuracy is given by $\alpha_5 = 0.68$, which value is denoted by α_5^{**}. As expected, when the cost of false negative errors is raised the threshold value of α_k is lowered. The classifier $C_5(\alpha_5)$ with $\alpha_5 = 0.68$ is denoted C_5^{**}, and gives a total cost-adjusted accuracy of

Table 4
Confusion matrix for classifier C_5^*

	$C_5^*(\alpha_5) = 1$	$C_5^*(\alpha_5) = 0$
$C(\theta_1, \ldots, \theta_{61}) = 1$	0.65	0.35
$C(\theta_1, \ldots, \theta_{61}) = 0$	0.04	0.96

Total accuracy 0.91.

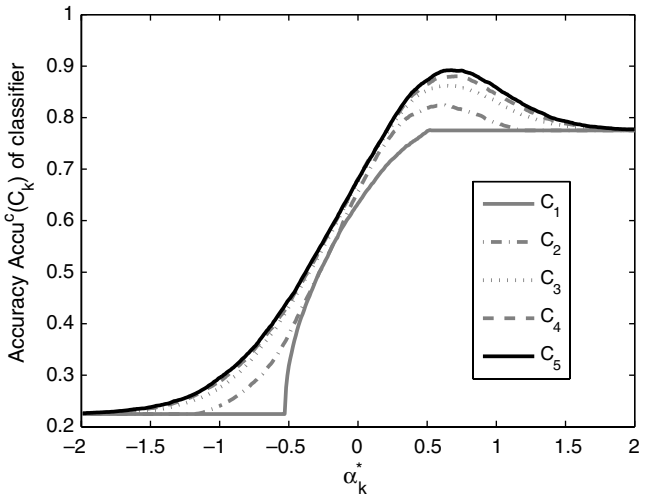

Fig. 10. Cost-adjusted accuracy of classifiers as a function of threshold value α_k^*.

$\text{Accu}^c(C_5^{**}) = 0.89$ and a total accuracy of $\text{Accu}(C_5^{**}) = 0.91$. Note that the cost-adjusted accuracy is used to determine the appropriate value of α_5^{**} but the true total accuracy $\text{Accu}(C_5^{**})$ should be used to evaluate classifier performance. The confusion matrix for classifier C_5^{**} (Table 5) shows that the introduction of a false negative cost $c_{\text{FN}} = 1.5$, which is greater than the false positive cost, decreases the false negative rate by 0.07 while increasing the false positive rate by only 0.02, and leaving the total accuracy essentially unchanged. For $c_{\text{FN}} = 1.5$ the false negative rate $\text{FN}(C_5^{**}) = 0.28$ remains uncomfortably high. Setting $c_{\text{FN}} = 3$ results in a false negative rate $\text{FN}(C_5^{**}) = 0.18$ and a total accuracy of 0.90. These results demonstrate the flexibility of the method, and the ability to reduce the false negative rate significantly without significant reduction in the total accuracy. These examples are illustrative, however, and, for a particular engineering application, the choice of the cost matrix must be made carefully.

Although attention here has focussed on a simple, two leaf decision tree operating on the single microstructural feature α_5, many other approaches to the classification of the training data are possible [15,16]. In closing the discussion of classifier development, then, comparison is made to three alternative classification approaches, namely linear regression, a decision tree and a support vector machine operating on the microstructural features $(\psi_1, \ldots, \psi_5)$. The linear regression, a hyperplane in $\mathbb{R}^5$, is defined by $s(\theta_1, \ldots, \theta_{61}) \approx s_{\text{lr}}(\psi_1, \ldots, \psi_5) = \omega_0 + \sum_{i=1}^{5} \omega_i \psi_i$, and the classification is made such that $C_{\text{lr}}(\psi_1, \ldots, \psi_5) = 1$ if $s_{\text{lr}}(\psi_1, \ldots, \psi_5) > s^*$, the threshold value of the effective stress in the central grain. The decision tree classifier, denoted by $C_{\text{dt}}(\psi_1, \ldots, \psi_5)$ is obtained using the software WEKA [17] using the J48 algorithm with pessimistic pruning applied. This decision tree differs from the one emphasized here in that it uses five input variables, resulting in a large decision tree, with several hundred nodes, even after pruning. In the decision tree emphasized here, only one node is used since the individual microstructural features have been combined into a single parameter, α_5, using the weighted sum of Eq. (26). Finally, and again using WEKA for the calculations, a linear support vector machine classifier $C_{\text{svm}}(\psi_1, \ldots, \psi_5)$ is trained and tested. The confusion matrices for these three classifiers are given in Tables 6–8. The results show that the regression model performs essentially equally as well as the classifier C_5^*. The five parameter decision tree C_{dt} has a somewhat lower total accuracy, and has a significantly higher false negative rate. The support vector machine classifier C_{svm} has nearly the same total accuracy as C_5^* but performs slightly worse in terms of false negative rate. Indeed any of these classifiers might be successfully applied to the problem at hand. The single parameter decision tree is the best performing, however, and is used in the following. It is also preferred because of its simplicity and the ease with which variable loss matrices can be incorporated into tree construction.

Table 5
Confusion matrix for classifier C_5^{**}

	$C_5^{**}(\alpha_5) = 1$	$C_5^{**}(\alpha_5) = 0$
$C(\theta_1, \ldots, \theta_{61}) = 1$	0.72	0.28
$C(\theta_1, \ldots, \theta_{61}) = 0$	0.06	0.94

Total accuracy 0.91.

Table 6
Confusion matrix for linear regression classifier C_{lr}

	$C_{\text{lr}} = 1$	$C_{\text{lr}} = 0$
$C(\theta_1, \ldots, \theta_{61}) = 1$	0.64	0.36
$C(\theta_1, \ldots, \theta_{61}) = 0$	0.04	0.96

Total accuracy 0.91.

Table 7
Confusion matrix for decision tree on $\psi_1, \ldots, \psi_5$

	$C_{\text{dt}} = 1$	$C_{\text{dt}} = 0$
$C(\theta_1, \ldots, \theta_{61}) = 1$	0.54	0.46
$C(\theta_1, \ldots, \theta_{61}) = 0$	0.05	0.95

Total accuracy 0.88.

Table 8
Confusion matrix for support vector machine on $\psi_1, \ldots, \psi_5$

	$C_{\text{svm}} = 1$	$C_{\text{svm}} = 0$
$C(\theta_1, \ldots, \theta_{61}) = 1$	0.61	0.39
$C(\theta_1, \ldots, \theta_{61}) = 0$	0.04	0.96

Total accuracy 0.91.

6. Application of classifier to large microstructures

The true value of a classifier such as that developed in the previous sections lies in providing rapid preliminary screening of heterogeneous materials. For example, in developing a finite element model of a large polycrystal,

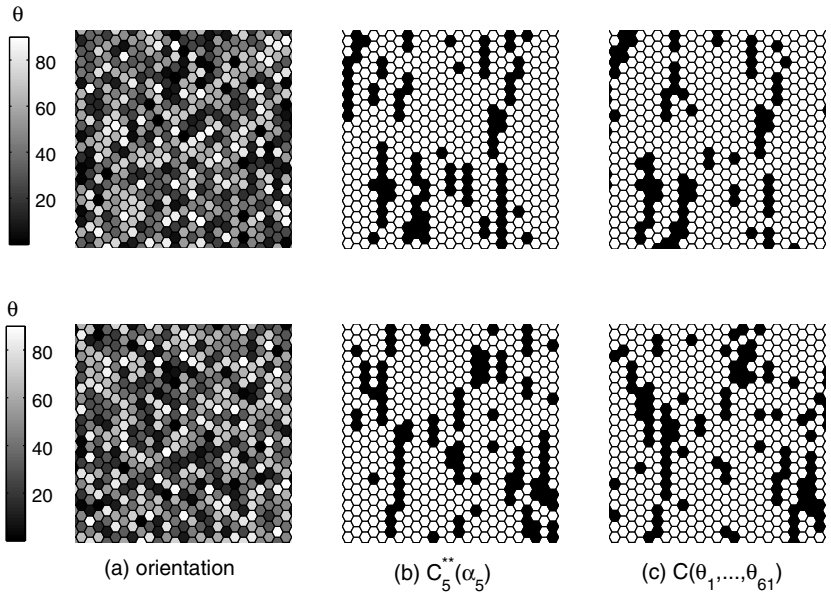

Fig. 11. Results of moving window classification of 1000-grain polycrystals. From left to right, for each row, the orientations, classifier result, and spring network result.

it might be desirable to use a finer mesh in regions where localization is likely to occur. A classifier approach can guide the analyst in determining which regions of a large material volume should be meshed with smaller or higher order elements. Similar reasoning can be applied to multiscale simulations in which the lower scales are instantiated only in regions where, for example, damage initiates. A classifier can also provide an initial, approximate, evaluation of the overall mechanical response of a microstructure, indicating, for example, whether large regions of the material domain are likely to be susceptible to damage.

To make the classifier useful in these kinds of contexts, a moving window approach is here defined that allows rapid scanning of a large polycrystal and identification of those grains that will experience elevated stress under boundary conditions similar to those used in developing the classifier. The test microstructures consist of 1000 grains and are subject to uniaxial extension with periodic displacement boundary conditions. In the moving window technique, each grain of the microstructure is treated as grain 1 of a 61-grain microstructure. The classifier C_5^{**} developed above is then applied to the orientations of these 61 grains. In this manner each grain is identified as critical or non-critical.

For comparison, a spring network simulation, similar to that used in developing the classifier, is performed on the 1000-grain microstructure. The average effective stress is calculated for each grain and grains are determined critical or non-critical according to $s > s^*$, the threshold effective stress. Thus, for each grain in the microstructure both $C_5^{**}(\alpha_5)$ and $C(\theta_1, \ldots, \theta_{61})$ are calculated. Here, despite the approximations inherent in the spring network model, $C(\theta_1, \ldots, \theta_{61})$ is considered to deliver the true class of the grain.

Two example results of the moving window classification of 1000-grain polycrystals are shown in Fig. 11. In the figure, the orientations are shown in greyscale in the left frame, and in the middle and right frames black crystals are critical. Although errors do exist, the overall match between the patterns of stress localization are quite consistent between the classifier and spring network results. The critical grains, in which the average von Mises stress exceeds a threshold, tend to occur in strings aligned with the principal loading axis. This can be attributed to two features of the material properties and mechanics of the problem. First, a string of grains, aligned with the principal loading axis, can occur that all have orientations leading to relatively high stiffness. This local stiffness will tend to attract load and result in locally higher stresses. Second, if an isolated grain has orientation such that it has high stiffness, it will tend to attract load, and, if the surrounding grains are of average stiffness, they will also experience somewhat elevated stress. The classifier, as implemented here in a moving window framework, is capable of identifying clusters of critical grains that are larger than the dimension of the patterns used in classification. Furthermore, that clusters of critical grains occur that are larger in dimension that the pattern used for classification should not be interpreted to mean that longer range interactions than are considered in pattern extraction are occurring. Rather, these clusters are a result of randomly occurring clusters of stiff grains.

7. Conclusions

The objective of this work is to develop a classifier-based method for predicting, approximately, the state of stress in a polycrystalline material, with random and heterogeneous material properties, subject to deterministic boundary conditions. The method presented here uses a decision tree

classifier operating on a reduced order representation of the material microstructure. The reduced order representation is based on the recognition of mechanically meaningful patterns in the spatial distribution of material properties.

Three theoretical developments are presented. First, the Sobol' decomposition of a function of many random variables is modified so that it can be applied to functions depending on variables that are uniform over an interval other than $[0,1)$. Second, the Sobol' indices, quantifying the contribution of individual input random variables to the variance of the response function, are used to identify the variables that should be retained in the reduced order representation. Specifically, they identify the subset of all nearby grains that should be used in classifying the response of a specific grain. Third, the first order Sobol' functions, which give the approximate dependence of the response function on the individual input variables, are used to develop a set of microstructural patterns that correspond to elevated average effective stress in a grain. By defining a type of projection of the microstructure onto these patterns, a single, scalar representation of the microstructural material properties is derived that correlates well with the response, the average effective stress.

A simple decision tree classifier is developed using this scalar representation of the microstructure that is able to predict whether the average effective stress in a grain will exceed a threshold value with an accuracy of approximately 0.91. This accuracy is achieved without resorting to any mechanics analysis such as finite element analysis, and the application of the classifier is extremely fast. The classifier is defined in such a way that the analyst is able to assign different costs to false negative (unconservative) and false positive (conservative) errors depending upon the particular application.

Finally, it is shown that this classifier can be used in a moving window algorithm to scan a relatively large (1000 grains) polycrystal subject to uniaxial extension, and determine with a high degree of accuracy which grains of the polycrystal will experience average effective stress above a specified threshold. Again, this classification is done without a high fidelity mechanics analysis and is extremely fast. This sort of moving window classification could prove useful in determining what subregions of a material volume should be instantiated at small scale in a multiscale simulation of material response. A subject of ongoing research is also whether it is possible to perform microstructural design and optimization using the classifier in place of traditional function evaluations such as finite element analysis, and whether the optimization can be performed directly in the reduced order space of microstructural descriptors.

Acknowledgement

The authors acknowledge financial support for this work from the US National Science Foundation through Grant #DMI-0423582, and Prof. T. Igusa for valuable discussions during the development of this work.

References

[1] T.C.T. Ting, Anisotropic Elasticity Theory and Application, Oxford University Press, 1996.
[2] J.D. Eshelby, The determination of the elastic field of an ellipsoidal inclusion and related problems, Proc. R. Soc. Lond. A241 (1957) 376.
[3] V.C. Prantil, J.T. Jenkins, P.R. Dawson, An analysis of texture and plastic spin for planar polycrystals, J. Mech. Phys. Solids 41 (8) (1993) 1357–1382.
[4] A. Ural, G. Heber, P.A. Wawrzynek, A.R. Ingraffea, D.G. Lewicki, J.B. Cavalcante Neto, Three-dimensional, parallel, finite element simulation of fatigue crack growth in a spiral bevel pinion, Gear Engrg. Fract. Mech. 72 (8) (2005) 1148–1170.
[5] A. Simone, C.A. Duarte, E. van der Giessen, A generalized finite element method for polycrystals with discontinuous grain boundaries, Int. J. Numer. Methods Engrg. 67 (2006) 1122–1145.
[6] A. Kumar, P.R. Dawson, Modeling crystallographic texture evolution with finite elements over neo-eulerian orientation spaces, Comput. Methods Appl. Mech. Engrg. 153 (1998) 259–302.
[7] G.B. Sarma, P.R. Dawson, Texture predictions using a polycrystal plasticity model incorporating neighbor interactions, Int. J. Plasticity 12 (8) (1996) 1023–1054.
[8] S.R. Arwade, M. Grigoriu, A probabilistic model for polycrystalline microstructures with application to intergranular fracture, ASCE J. Engrg. Mech. 130 (2004) 997–1005.
[9] H. Liu, S.R. Arwade, T. Igusa, Random composites characterization using a classifier model, ASCE J. Engrg. Mech. 133 (2007) 129–140.
[10] I. Sobol', S. Kurachenko, Global sensitivity indices for nonlinear mathematical models, Rev., Wilmott Mag. 1 (2005) 56–61.
[11] B. Sudret, Global sensitivity analysis using polynomial chaos expansion, in: Proceedings of the Fifth International Conference on Computational Stochastic Mechanics, Rhodes, Greece, 2006.
[12] R.J. Asaro, Geometrical effects in the inhomogeneous deformation of ductile single crystals, Acta Metall. 27 (1979) 445–453.
[13] T. Iwakuma, S. Nemat-Nasser, Finite elastic–plastic deformation of polycrystalline metals, Proc. R. Soc. Lond. A394 (1984) 87–119.
[14] M.M. Rashid, Texture evolution and plastic response of two-dimensional polycrystals, J. Mech. Phys. Solids 40 (5) (1992) 1009–1029.
[15] V.N. Vapnik, Statistical Learning Theory, Wiley, New York, 1998.
[16] T. Hastie, R. Tibshirani, J. Friedman, The Elements of Statistical Learning, Springer, New York, 2001.
[17] I.H. Witten, F. Elbe, Data Mining: Practical Machinelearning Tools and Techniques, second ed., Morgan Kauffman, San Francisco, 2005.